Review

Atomic Processes, Including Photoabsorption, Subject to Outside Charge-Neutral Plasma

Tu-Nan Chang [1,*]**, Te-Kuei Fang** [2]**, Chensheng Wu** [3] **and Xiang Gao** [4,*]

[1] Department of Physics, University of Southern California, Los Angeles, CA 90089-0484, USA
[2] Department of Physics, Fu Jen Catholic University, Taipei 242, Taiwan; 051420@mail.fju.edu.tw
[3] Institution of Applied Physics and Computational Mathematics, Beijing 100088, China; wuchensheng89@foxmail.com
[4] Beijing Computational Science Center, Beijing 100193, China
[*] Correspondence: tnchang@usc.edu (T.-N.C.); xgao@csrc.ac.cn (X.G.)

Abstract: We present in this review our recent theoretical studies on atomic processes subject to the plasma environment including the α and β emissions and the ground state photoabsorption of the one- and two-electron atoms and ions. By carefully examining the spatial and temporal criteria of the Debye–Hückel (DH) approximation based on the classical Maxwell–Boltzmann statistics, we were able to represent the plasma effect with a Debye–Hückel screening potential V_{DH} in terms of the Debye length D, which is linked to the ratio between the plasma density N and its temperature kT. Our theoretical data generated with V_{DH} from the detailed non-relativistic and relativistic multiconfiguration atomic structure calculations compare well with the limited measured results from the most recent experiments. Starting from the quasi-hydrogenic picture, we were able to show qualitatively that the energy shifts of the emission lines could be expressed in terms of a general expression as a function of a modified parameter, i.e., the reduced Debye length λ. The close agreement between theory and experiment from our study may help to facilitate the plasma diagnostics to determine the electron density and the temperature of the outside plasma.

1. Introduction

Reliable data for many of the atomic processes subject to the outside charge-neutral plasma are important for the numerical modeling of the evolution of many processes for the energy-related controlled fusion program and also some of the astrophysical systems [1–4]. With the help of the high-speed large-scale computational facilities, currently, the theoretical atomic structure calculations by including all the electron–electron interactions between atomic electrons are capable of generating highly reliable atomic data in close agreement with the experimental observations in the plasma-free environment. However, a detailed theoretical understanding of the atomic process in the plasma environment would need to include the practically unattainable efforts to cover the long-range interactions between the atomic electrons and all the positively charged ions and the negatively charged electrons in the plasma. Over the years, by including the interactions between the atomic electrons and the outside plasma, attempts have been made with somewhat detailed theoretical methods [5–13] to generate data that may understand the limited experimental measurements. One such example is the application of the ion sphere (IS) approach [8–10]. Whereas the calculated redshifts of the α emission of the He-like Al ion based on an analytical IS model [8,9] are in agreement with the recent picosecond time-resolved measurement [14], its estimated redshifts at a fixed temperature are substantially greater than the measured data from a high-resolution satellite line-free measurement of the β line of the He-like Cl ions (see Figure 4 of [15]). In addition, shortly after the He-like Cl ion measurement, the estimated energy shift from an average atom ion sphere (AIS) model calculation was

reported to be in good agreement [10]. However, the subsequent application of this AIS model to the α emission of the He-like Al ion has led to redshifts substantially smaller than the earlier experimentally observed data (see Figure 2 of [16]). The disagreement between the IS theories and experiments likely results from the less-than-adequate representation of the interaction between the outside plasma and the atomic electrons.

The main objective of this review is to summarize a series of recent studies based on the Debye–Hückel (DH) model, proposed before the quantum mechanics was fully developed [17], on the atomic processes in the plasma environment. The DH approximation, based on the classical Maxwell–Boltzmann statistics for an electron–ion collision-less plasma, is best known to work for the gas-discharged plasma at relatively low density [18]. To apply the DH approximation to the atomic processes subject to plasma with higher density, one needs to consider two important key criteria. First, temporally, the time scale of the atomic process (e.g., lifetime) should be substantially different from its correlation time t_p, or the inverse of the plasma frequency ($f_p = 8.977 \times 10^3 \, N^{1/2}$Hz) of the outside plasma with density N. For a plasma with its density of the order of 1×10^{22} cm^{-3}, t_p is of the order of 10^{-15} s. This is substantially shorter than the lifetime T_{2p} of the Lyman-α emission line of the hydrogen atom from its $2p$ state, which is of the order of nanoseconds, or more precisely, 1.6 ns. It is also known that T_{2p} scales as the inverse of Z^4, and it would decrease to a similar order of magnitude of t_p as Z for the H-like ion increases up to about 18. The values of T_{2p} will again be substantially shorter than t_p with Z greater than 50. The other important time factor is the time for an electron moving around the nucleus. Again, take the Lyman-α emission line of the hydrogen atom as an example: the time for the $2p$ electron moving around the nucleus is about 10^{-15} s, which is similar for t_p. Since this revolving speed scales as Z^2 and it would be an order of magnitude higher than t_p with $Z > 5$, as a result, the DH approximation works for the Lyman-α emission line of the H-like ions only with Z between six and eighteen or greater than fifty. Second, spatially, the atomic orbitals involved in the transition should only be affected marginally by the outside plasma to retain most of their atomic characteristic. For example, for the transitions involving the electron in its ground state with the radius of its electron orbital sufficiently short in range, the contribution to the overlapping transition matrix between the lower and upper atomic orbitals of the atomic processes is mostly from a critical interacting region with the influence of the outside plasma included and the amplitude of the lower atomic orbital mostly non-zero. In other words, the DH approximation should only be applied to those transitions involving the ground state or the low-n states. Detailed discussions about these two key criteria were also given elsewhere [19–23]. In essence, the complicated many-body interaction between the atomic electrons and the outside charge-neutral plasma is effectively represented by a simple potential $V_{DH}(r)$ depending on two key parameters. The first one is the Debye length D, which can be expressed in the Bohr radius a_0 in terms of the ratio of the temperature kT and the electron density N (in units of eV and 10^{22} cm^{-3}, respectively) of the outside plasma as $D = 1.4048 \, (kT/N)^{1/2}$ [17,18]. For the plasma-free environment, the density N equals zero and D goes to infinity. Effectively, the Debye length D, which appears in the form of $e^{-r/D}$ or a Debye screening, modifies the attractive nuclear interaction $-Z/r$ in the potential V_{DH} due to the outside plasma. The second one is an ad hoc parameter, i.e., the radius A of the Debye sphere, which separates the plasma-induced Debye potential V_{DH} outside the Debye sphere and the slightly modified close-in region where the atomic characteristic dominates. More details on these two parameters, as well as the original approach of the DH approximation leading to the effective potential V_{DH} are presented in Section 2. A brief summary of the multiconfiguration non-relativistic and relativistic calculational procedures is also given in Section 2.

Due to its simplicity, the DH model has been applied extensively to study the atomic processes subject to the outside plasma [24–35]. As we show in Section 2, the atomic electrons are subject to an effective DH potential derived from the Gauss theorem by assuming an infinitely heavy nuclear charge Z located at $r = 0$ with screening from the fast free-moving plasma electrons of high mobility. In contrast, with the relatively low

mobility of the plasma ions, one could not assume a substantial presence of the plasma ions between the fast-moving atomic electrons. In other words, there is little theoretical justification to apply the Debye screening to the two-body Coulomb interaction between atomic electrons. By including the Debye screening, which effectively reduces the Coulomb repulsive interaction between atomic electrons, a high-precision theoretical calculation has indeed led to the spurious conclusion that the only known bound state of H^- between two loosely bound electrons would stay bound even in the presence of a strong outside plasma [34,35].

We review in detail in Section 3 our recent applications of the DH approximation to the α-emission lines of the H-like and He-like ions subject to the outside plasma [20–23]. Our calculated redshifts in transition energy are in agreement both with the experimentally observed data [14,15,36], as well as the results from some of the more elaborate simulations based on the quantum mechanical approaches [5–13]. Interestingly, our studies led to a simple scaling feature for the redshifts of the transition energy and the oscillator strength as functions of a related parameter, the *reduced Debye length* $\lambda = Z_{eff}D$, defined as the product of the Debye length D and the effective nuclear charge $Z_{eff} = Z - 1$ of the atomic ion [22,23]. Specifically, the ratio between the shifts in the transition energy $\Delta\omega$ and the plasma-free transition energy ω_0, i.e., $R_\omega = \Delta\omega/\omega_0$, could be expressed by a simple polynomial in terms of this new parameter λ for all ions with applicable nuclear charge Z. Indeed, our calculations with the non-relativistic and the relativistic multiconfiguration calculations have confirmed such a general scaling feature (e.g., see Figure 5 of [21] and Figure 1 of [23]). By introducing this new parameter λ, we were able to focus our application of this slightly modified DH approximation for the general features of the atomic transition data that could be extended to all applicable ions from a single theoretical calculation.

We focus our review on the atomic photoabsorption from the ground state of the one- and two-electron atoms in Section 4. First, we should point out that we modified the term photoionization from our originally published works to photoabsorption due to the realization that the speed of the outgoing ionized electron after the absorption of the incoming photon is generally less than the speed of the outside plasma electrons, and experimentally, the resulting outgoing photoelectron could not be measured, such as the one in a plasma-free photoionization experiment. The application of the DH approximation would also be limited to the process involving mostly the ground state of the target atoms to meet the spatial criterion when the transition rate is only affected by the overlap between the initial and final state wavefunctions at small r when the plasma effect is well represented by the V_{DH}, as we discussed earlier.

Finally, we summarize briefly in Section 5 the implications of our studies and the further interplays between the theoretical estimate of the atomic data based on the application of the DH approximation and the more advanced experimental works. In particular, to fully take advantage of the general feature in terms of the reduced Debye length for the transition energy shifts as a plasma diagnostic possibility, further high-precision experiments are necessary for a better determination of the range of the radius A of the Debye sphere.

2. Debye–Hückel Approximation and the Calculational Procedure

The theoretical methods were presented in detail in our recent works [21,23]. In this section, we repeat some of the key equations to facilitate a self-contained discussion.

Based on the original Debye–Hückel model [17], the potential $V_o(r)$ for an electron–ion collision-less plasma at a distance r far from the atomic nucleus Z outside a Debye sphere of radius A can be derived from Poisson's equation based on the Gauss law:

$$\nabla^2 V_o(r) = -\frac{\rho(r)}{\epsilon}, \quad r \geq A, \tag{1}$$

where ϵ is the dielectric constant of the electron–ion gas and ρ is its total charge density at r. Starting from the Boltzmann distribution and assuming a charge density ρ_o and a zero potential at $r = \infty$, the charge densities of the negative charge $-q$ and the equal

positive charge q at r could be expressed as $\rho_-(r) = \rho_o e^{qV_o(r)/kT}$ and $\rho_+(r) = \rho_o e^{-qV_o(r)/kT}$, respectively, where k is the Boltzmann constant and T the absolute temperature. The total charge density at r is then given by:

$$\rho(r) = \rho_o(e^{-\frac{qV_o(r)}{kT}} - e^{\frac{qV_o(r)}{kT}}) = -2\rho_o \ \sinh\ (\frac{qV_o(r)}{kT}). \tag{2}$$

Additionally , if qV_o is relatively small compared to kT, Equation (2) for the potential in the outer region of the Debye sphere could then be approximated by the *linear* Poisson–Boltzmann equation, i.e.,

$$\bigtriangledown^2 V_o(r) = (\frac{1}{D^2})V_o(r), \quad r \geq A, \tag{3}$$

where $D > A$ is the Debye length in Bohr radius a_0 defined in terms of the ratio of the density N ($\sim q\rho_o$) in units of 10^{22} cm^{-3} and the temperature kT in units of eV of the outside plasma given earlier, i.e.,

$$D = 1.4048(\frac{kT}{N})^{1/2}a_0. \tag{4}$$

The potential inside the Debye sphere is derived from the Gauss law, i.e.,

$$V_i(r < A) = -\frac{Ze^2}{r} + Constant. \tag{5}$$

By matching V_o and V_i and their first-order derivatives at $r = A$, one obtains [20,37,38]:

$$V_{DH}(r) = \begin{cases} V_i(r) = -Ze^2(\frac{1}{r} - \frac{1}{D+A}), & r \leq A \\ \\ V_o(r) = -Ze^2(\frac{De^{A/D}}{(D+A)})\frac{e^{-r/D}}{r}, & r \geq A. \end{cases} \tag{6}$$

In the limit when $A \to 0$, Equation (6) reduces to the screened Coulomb potential $-(Z/r)e^{-r/D}$, similar to the Yukawa potential in nuclear physics. From Equation (6), the DH model, or the DH potential V_{DH}, depends on two important parameters, as we discussed earlier in Section 1. The first one is the Debye length D, which goes to infinity when the density N equals zero for the plasma-free environment. The second one is an ad hoc parameter, i.e., the radius of the Debye sphere A, which separates the plasma-induced Debye potential V_{DH} outside the Debye sphere and the slightly modified close-in region where the atomic characteristic dominates.

The consequence of the less-attractive Debye potential V_{DH} is that all the atomic levels will experience an up-lifting in energy. Qualitatively, the change in the transition energy $\Delta\omega$ from its plasma-free transition energy ω_o for an atomic transition subject to the outside plasma depends on the decrease or increase of the difference in the relative energy shifts of the initial and final state of the transition. For the intershell transitions, although the percentage change of the orbital energy is larger for an electron with a larger principal quantum number n due to the stronger outside plasma effect, its small plasma-free orbital energy actually makes the net energy change smaller than the one for the electron with a smaller n; thus, the transition energy is redshifted. On the other hand, for the intrashell transitions, the involved electrons are from the orbitals with the same n; the change in energy is greater for the one with larger orbital angular momentum. However, additional factors such as the interplay between the electron–electron correlation and the relativistic interactions may also affect the relative energies of the initial and final states. As a result, dependent on the individual transition, the transition energy could either be blueshifted or redshifted.

Another interesting immediate consequence of the DH potential V_{DH} is that the ratio $R = \Delta\omega/\omega_o$ for the α emission line for the H-like ion depends on a single parameter, i.e., the reduced Debye length, defined as $\lambda = ZD$. Qualitatively, the energy shift of the emission line subject to the outside plasma $\Delta\omega_\alpha$ is given approximately by the difference in the energy corrections between the initial and final H-like orbitals due to the difference in the Coulomb potential and the screened Coulomb potential, i.e., $\Delta V_D = \frac{Z}{r}(1 - e^{-r/D})$. This can be estimated by the difference of the expectation values of $\Delta_{1s} = < 1s \mid \Delta V_D \mid 1s >$ and $\Delta_{2p} = < 2p \mid \Delta V_D \mid 2p >$, or given analytically by [21]:

$$\Delta\omega_\alpha(D) \approx \Delta_{1s}(D) - \Delta_{2p}(D) = Z^2 \left[\frac{3}{4} - (1 + \frac{1}{2\lambda})^{-2} + \frac{1}{4}(1 + \frac{1}{\lambda})^{-4} \right]. \tag{7}$$

Since the plasma-free transition energy of the Lyman-α line ω_0 is also proportional to Z^2, the ratio $R = \Delta\omega/\omega_0$ is a function of λ only, or more conveniently, R could be expressed by a simple polynomial in terms of the reduced Debye length λ for all ions with applicable nuclear charge Z. Effectively, we demonstrated a simple scaling feature for the plasma-induced transition energy shifts in terms of the reduced Debye length λ.

The theoretical results presented in this review were carried out with the multiconfiguration approaches, both non-relativistically and relativistically. The non-relativistic results were calculated with the B-spline-based configuration interaction (BSCI) approach with a complete two-electron basis corresponding to both negative and positive energy atomic orbitals. The individual one-electron atomic orbitals were generated from an effective one-electron Hamiltonian $h_o(r, D)$, i.e.,

$$h_o(r; D) = \frac{p^2}{2m} + V_{DH}(r; D), \tag{8}$$

where p is the momentum of the electron and $V_{DH}(r; D)$ is given by Equation (6). The N-electron Hamiltonian for an atom in the plasma environment is expressed in terms of $h_o(r; D)$ as:

$$H(r_i, r_j, \cdots ; D) = \sum_{i=1,N} h_o(r_i; D) + \sum_{i>j}^{N} \frac{e^2}{r_{ij}}, \tag{9}$$

where $r_{ij} = \mid \vec{r_i} - \vec{r_j} \mid$ represents the separation between the atomic electrons i and j. The state wave functions for the upper and lower states of the transition, ϕ^U and ϕ^L with energies ϵ^U and ϵ^L, respectively, were calculated by diagonalizing the Hamiltonian matrix with the basis set of the multiconfiguration two-electron orbitals discussed earlier and following the numerical procedure detailed elsewhere [39–42]. The energy of the emission line under the external plasma environment in terms of the Debye length D is given by the difference of the energies between the upper (U) and the lower (L) state, i.e.,

$$\omega(D) = \epsilon^U(D) - \epsilon^L(D). \tag{10}$$

The energy of the emission line in the absence of the external plasma is given by $\omega_o = \omega(D = \infty)$, and the transition energy shift $\Delta\omega$ is thus given by:

$$\Delta\omega(D) = \omega_o - \omega(D). \tag{11}$$

The details of the theoretical and calculational procedures leading to the oscillator strength were given in Section 2.4 of [39].

For the relativistic calculation of an N-electron ion with nuclear charge Z subject to the outside plasma, its N-electron Hamiltonian H_{DH} can be expressed as:

$$H_{DH} = H_{DC} + \sum_{i=1}^{N} V_d(r_i, D), \quad V_d(r_i, D) = \frac{Z}{r_i} + V_{DH}(r_i), \tag{12}$$

where H_{DC} is the the well-known Dirac–Coulomb Hamiltonian in the absence of the plasma environment, i.e.,

$$H_{DC} = \sum_{i=1}^{N} [\, c\,\vec{\alpha}\cdot\vec{p}_i + (\beta - 1)mc^2 - \frac{Z}{r_i}\,] + \sum_{i>j}^{N} \frac{e^2}{r_{ij}}, \tag{13}$$

where $\alpha_k = \begin{pmatrix} 0 & \sigma_k \\ \sigma_k & 0 \end{pmatrix}$ with $k = (1,2,3)$, σ_k is the Pauli 2×2 matrix, and $\beta = \begin{pmatrix} I & 0 \\ 0 & -I \end{pmatrix}$ with I the 2×2 unit matrix.

The energies E^{Γ} and the their corresponding state functions (ASFs) $|\Gamma PJM\rangle$ of the upper and lower states of the atomic process are derived from:

$$H_{DH}|\Gamma PJM\rangle = E^{\Gamma}|\Gamma PJM\rangle \tag{14}$$

with P the parity, J the total angular momentum, M its magnetic quantum number, and Γ all other information to define the ASF uniquely. The ASFs are N-electron eigenstate wave functions, which are the linear combinations of the configuration state functions (CSFs) with the same P, J, and M, namely,

$$|\Gamma PJM\rangle = \sum_{i=1}^{n_e} C_i^{\Gamma} |\gamma_i PJM\rangle, \tag{15}$$

where C_i^{Γ} is the expansion coefficient and γ_i represents all other information to define the CSF uniquely. The CSFs, $|\gamma_i PJM\rangle$, which form a basis set for an N-electron atomic system, are linear combinations of the Slater determinants of the atomic orbital wave functions (AOs) corresponding to the electron configurations included in the calculations. The electron correlation effects were taken into account by diagonalizing the relativistic H_{DH} with a quasi-complete basis in a revised multiconfiguration Dirac–Fock (MCDF) approach. The basis consists of the spectroscopic AOs (with $n - l - 1$ fixed nodes) and pseudo AOs (without fixed nodes). Both AOs are specified by the principal quantum number n, the orbital angular momentum l, and the total angular momentum j. The number of spectroscopic orbitals depends on the requirement of specific physical problem, i.e., the degrees of excitations of target ions, whereas the number of pseudo orbitals is determined by the desired accuracies. The atomic orbitals (AOs) were optimized using the GRASP-JT version based on the earlier GRASP2K codes [43,44]. The details of the calculational schemes have been presented elsewhere [45–47]. With the ASFs calculated with and without the outside plasma and under the dipole long-wavelength approximation, the oscillator strength of transition between atomic states can be expressed as the product of the transition energy $\omega_{\alpha\beta}$ and the square of the transition matrix element in the length gauge as:

$$g_{\alpha}f_{\alpha\beta} \sim \omega_{\alpha\beta} \cdot |\sum_{i,j} C_i^{\Gamma_{\alpha}} C_j^{\Gamma_{\beta}} \langle \gamma_i P_i J_i M_i |\hat{r}| \gamma_j P_j J_j M_j \rangle|^2, \tag{16}$$

where $\langle \gamma_i P_i J_i M_i |\hat{r}| \gamma_j P_j J_j M_j \rangle$ are the dipole transition matrix elements.

For the relatively light He-like ions, the relativistic effect is small, and the results from our non-relativistic and relativistic calculations are in close agreement with each other, as shown previously [21]. As a result, the discussion in Section 3 was mostly based on our non-relativistic calculation. We should also point out that the close agreement between two very different calculation approaches (i.e., the non-relativistic BSCI approach with the spin–orbit interaction included and the relativistic GRASP2K approach with the optimized atomic orbitals in its quasi-complete basis) suggests that the electron–electron correlation was fully included in our study.

For the atomic processes involving the continuum such as the atomic photoabsorption, the detailed expressions for its cross-section σ in terms of the excitation energy and the oscillator strength (either in the length or velocity gauge) were given in detail elsewhere [39,40].

With the state wave functions generated following our discussion presented above, our calculated plasma-free photoabsorption cross-sections σ with either the length or velocity approximation for the He-like atomic systems are generally in agreement to within 1–2%. The agreement at such a level suggests again that the electron–electron correlation between atomic electrons was taken into account fully in our theoretical calculation.

3. Plasma Effects on H-like and He-like Ions

Our first attempt to apply the DH approximation to the shift of the transition energy $\Delta\omega$ subject to the outside plasma started with the Lyman-α line of the one-electron H-like ions. Our main objective was to find if the estimated $\Delta\omega$ based on the DH model would agree with the quantitatively measured redshift of 3.7 ± 0.7 eV for the H-like Al^{12+} ion from the laser-generated plasma at temperature 300 eV with its density of $(5–10) \times 10^{23}$ cm^{-3} [36]. We chose in our calculation the Debye radius as the product of the radius of the 1 s orbit a_o/Z and a size parameter η, i.e., $A = (\eta/Z)a_o$. For a H-like ion, we simply solved the one-electron Hamiltonian Equation (8) with a given D corresponding to a pair of (kT, N) and evaluated the resulting redshift. Figure 1 compares the experimental redshift to our calculated results with four different size parameters at $\eta = 0$, 1, 1.5, and 2. With the experimental density extended from $5–10 \times 10^{23}$ cm^{-3}, all our theoretically estimated redshifts with different η compared well with the observed value of 3.7 ± 0.7 eV. It also turned out that our estimated redshifts with $\eta = 0$ for the Lyman-α emission of H-like Ne^{9+} ion at 500 eV are in agreement with the theoretical result of an earlier QMIT (quantum mechanical impact theory) study by Nguyen et al. [5,6], which included the effect of total ion polarization and considered as the upper limit for the redshift. As pointed out by Nguyen et al., their limiting result was about 20% greater than the result from an earlier quantum mechanical treatment by Davis and Blaha [7] with only a partial account of the ion charge density. Interestingly, the estimate by Davis and Blaha is in agreement with our calculated redshift with $\eta = 1.0$. More discussion was presented earlier in detail in Figure 4 of [20].
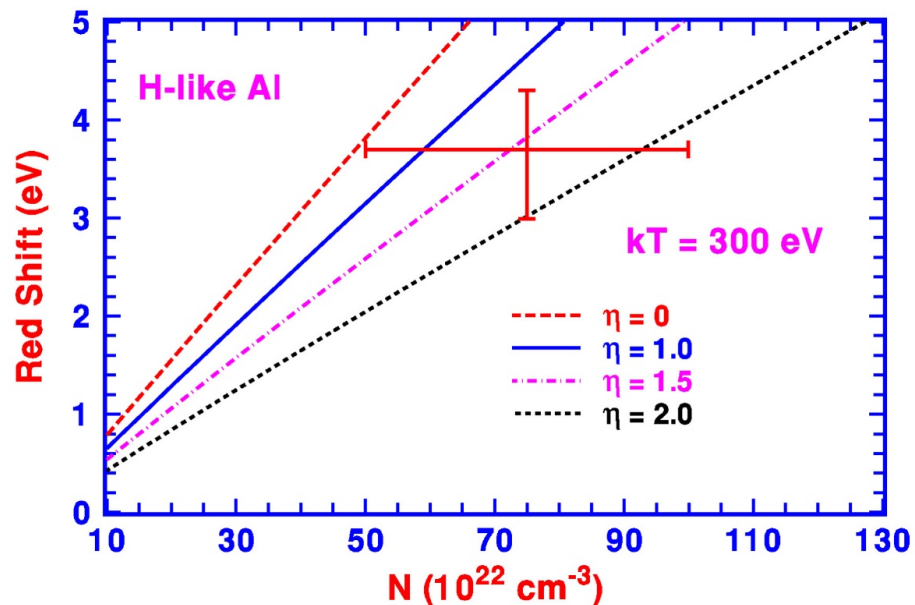
Figure 1. Comparison between the experimentally measured Lyman-α redshift of the H-like Al ion [36] with the theoretical estimations with the radius of the Debye sphere A in terms the size parameters $\eta = 0$, 1, 1.5, and 2.

Encouraged by the agreement between our theoretical results on the Lyman-α emission of the H-like ions and the experimental observation, as well as other more detailed theoretical calculations, we moved on to study the α and β emissions of the He-like ions. With the

electron–electron correlations between the atomic electrons taken into account fully based on the non-relativistic and relativistic multiconfiguration atomic structure calculations outlined in Section 2, we carried out calculations for the He-like Ne, Al, and Ar ions with the radius of the Debye sphere given by $A = \eta < r >_g$, where $< r >_g = \langle 1s^2\,{}^1S|r|1s^2\,{}^1S \rangle$ is the average radius of the ground state of He-like ions and η is a size parameter. Our calculations led to (i) the plasma-free transition energies ω_0 for all three He-like Ne, Al, and Ar ions, in close agreement with the NIST values [48], and (ii) the ratio R shown in Figure 2 between the energy shift $\Delta\omega$ and the plasma-free ω_o, which follows a nearly universal curve for each size parameter η as a function of the reduced Debye length λ for all He-like ions with Z meeting the spatial and temporal criteria of the DH approximation. This is qualitatively consistent with what we already pointed out earlier in Section 2, following the quasi-hydrogenic picture based on Equation (7). For the He-like ions with relatively low Z, the relativistic interactions are small, and indeed, this was confirmed by the nearly identical values R for the He-like O^{6+} ion between the non-relativistic and relativistic results shown previously in Figure 5 of [21]. For the intermediate Z, the DH approximation did not work due to the spatial and temporal criteria, as we pointed out earlier. As Z increases further, the DH model should apply again, and the effect of the relativistic interaction was clearly shown for the heavier He-like Yb and Au ions as the values of R deviated substantially from the ones for He-like O ion, shown also in Figure 5 of [21]. Our discussion below for the plasma effects on ions with relatively low Z was mostly based on the data from our non-relativistic calculations.
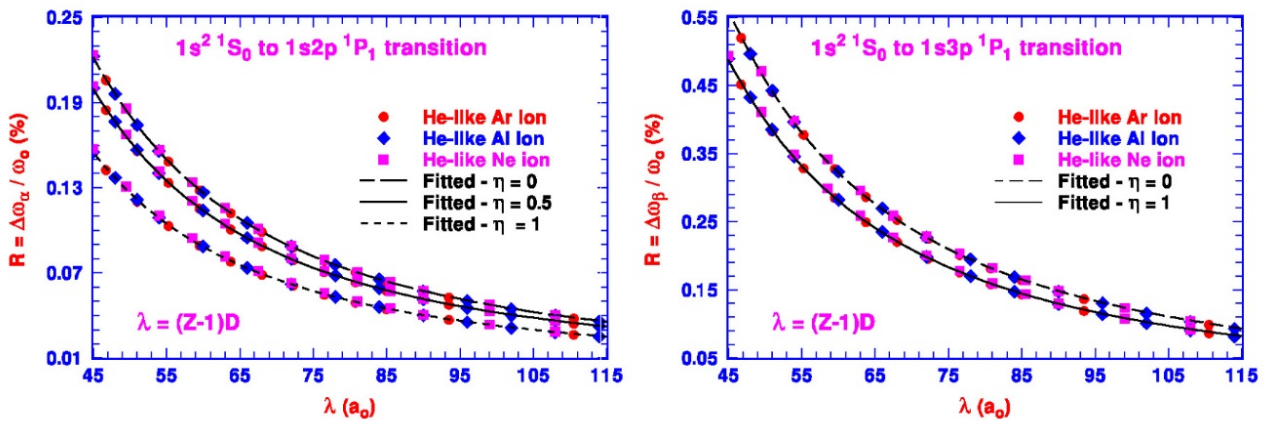
Figure 2. The universal behavior of the calculated R as functions of the reduced Debye length λ for three He-like ions and their comparison to the fit ratio R given by Equation (17) with the coefficients given in Table 1.

The nearly universal dependence of the calculated R on λ for different He-like ions shown in Figure 2 could be expressed more conveniently with a simple polynomial in terms of three numerically fit coefficients a, b, and c as:

$$R(\lambda; a, b, c) = a + b/\lambda + c/\lambda^2, \tag{17}$$

To estimate the ratio R for other He-like ions, we first took the average of the fit coefficients a_Z, b_Z, and c_Z from the calculated R of the three ions with individual Z shown in Figure 2. Corresponding to each size parameter η, the coefficients listed in Table 1 are the average over the individually fit coefficients for the three He-like ions, i.e., $a_\eta = (a_{Ne^{8+}} + a_{Al^{11+}} + a_{Ar^{16+}})/3$ for the α and β emission lines of the He-like ions. As expected, the R values generated with the coefficients listed in Table 1 and Equation (17) agree well with the calculated R, as shown by the two plots of Figure 2.

Theoretically, the ratio R should go to zero as the energy shift approaches zero when λ or the Debye length D goes to infinity. With the two coefficients c and b several orders of

magnitude larger than the small, but non-zero coefficient a, one could identify the coefficient a as the numerical uncertainty of the theoretically estimated ratio R. Based on Equation (17) and the fit coefficients listed in Table 1, it is straightforward to estimate the transition energy shifts $\Delta\omega$ following three simple steps for the α and β emission lines for any He-like ions with Z between six and eighteen. First, one starts from a specific reduced Debye length $\lambda = (Z-1)D$ with D determined from Equation (4) for a pair of plasma density N and temperature kT. Second, we proceeded to calculate the ratio R from Equation (17) for each λ with the coefficients listed in Table 1. In the third step, the estimated energy shift $\Delta\omega$ corresponding to this specific pair of N and kT is given by $\Delta\omega(N,kT) = R(\lambda)\omega_0$ with ω_0 the plasma-free transition energy. Following this simple procedure, the estimated redshifts $\Delta\omega(eV)$ for the α and β emission lines of the He-like Cl ion at 600 eV and 800 eV as functions of N in unit of 10^{23} cm^{-3} with three size parameters $\eta = 0, 0.5$, and 1 are presented in Table 2. The top plot of Figure 3 shows good agreement between our estimated redshifts listed in Table 2 for the β emission line of the He-like Cl ion and the experimental data from the recent high-resolution satellite line-free measurement [15]. Similar good agreement is also shown in the bottom plot of Figure 3 between our calculated redshifts of the α emission line of the He-like Al ion and the results of the recent picosecond time-resolved measurement [14]. It is interesting to note that the fit coefficients c listed in Table 1 are about three orders of magnitude greater than the coefficient b and seven orders greater than the coefficient a. Therefore, the estimated energy shifts should be dominated by the term c/λ^2, or proportional to the ratio N/kT. This is consistent with what is shown in Figure 3: the nearly linear dependence of the redshift $\Delta\omega$ as a function of the plasma density N at a fixed temperature kT. We should point out that this linear dependence is also consistent with the analytical expression derived by Li and Rosmej in their IS model [8,9]. On the other hand, the same reasoning based on the DH approximation that the energy shift should vary as N/kT suggests that at a constant density N, $\Delta\omega$ should vary linearly as the inverse of the temperature, i.e., $1/kT$, such as the ones shown in the bottom plot of Figure 4. This is different from the analytical expression from the IS model of Li and Rosmej [8,9], which suggests a temperature dependence of $(1/kT)^{1/2}$.

Table 1. Fit average coefficients a, b, and c in $A(e) = A \times 10^e$ for the α and β emission lines of the He-like ions with the size parameters $\eta = 0, 0.5$, and 1 (corresponding to the R in percentage).

	The α Emission Line of the He-like Ions			**The β Emission Line of the He-like Ions**		
η	a	b	c	a	b	c
0.0	$-9.08030\,(-5)$	$2.96178\,(-1)$	$4.37256\,(2)$	$-4.19761\,(-4)$	$1.45386\,(0)$	$1.07289\,(3)$
0.5	$-8.89317\,(-5)$	$2.90274\,(-1)$	$3.92346\,(2)$	$-4.17651\,(-4)$	$1.44754\,(0)$	$1.02662\,(3)$
1.0	$-8.01969\,(-5)$	$2.63109\,(-1)$	$3.02430\,(2)$	$-4.08090\,(-4)$	$1.41677\,(0)$	$9.26831\,(2)$

Table 2. The redshifts $\Delta\omega(eV)$ of the β emission line for the He-like *Cl* ion derived from the fit coefficients listed in Table 1 at 600 eV and 800 eV as functions of the plasma density N in (10^{23} cm^{-3}) with the size parameters $\eta = 0, 0.5$, and 1.

$N(10^{23}$ cm$^{-3})$	**$kT = 600$ eV** $\Delta\omega$ **(eV)**			**$kT = 800$ eV** $\Delta\omega$ **(eV)**		
	$\eta = 0$	$\eta = 0.5$	$\eta = 1$	$\eta = 0$	$\eta = 0.5$	$\eta = 1$
1.5	2.058	1.982	1.813	1.579	1.521	1.394
2.5	3.313	3.186	2.908	2.532	2.436	2.227
3.5	4.550	4.373	3.986	3.469	3.336	3.044
4.5	5.777	5.549	5.053	4.396	4.226	3.852
5.5	6.996	6.718	6.113	5.318	5.109	4.654
6.5	8.210	7.882	7.168	6.235	5.989	5.451
7.5	9.419	9.041	8.218	7.148	6.864	6.245
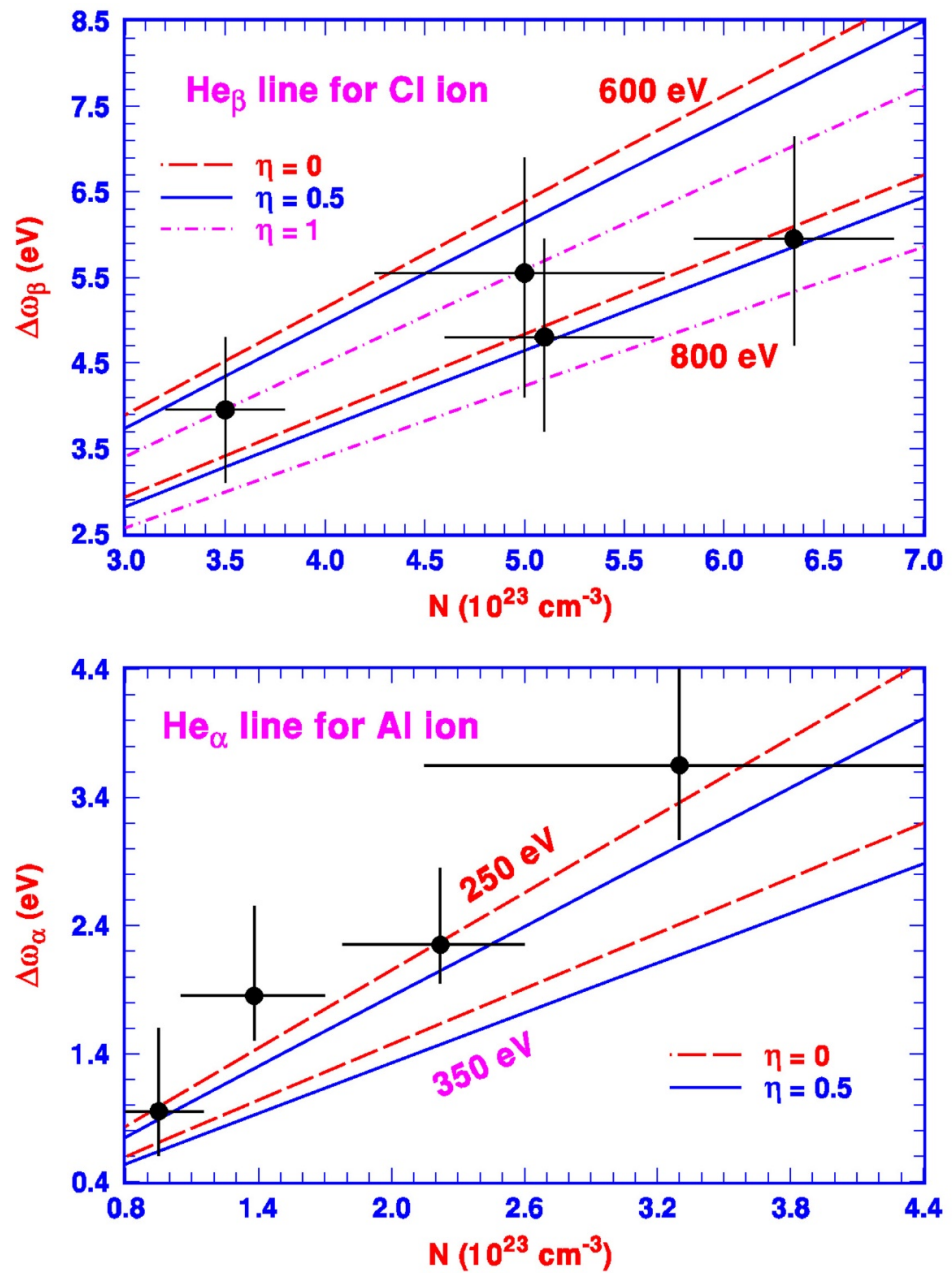
Figure 3. The comparison between the redshifts $\Delta\omega$ for the β and α emissions of the He-like ions estimated based on the DH approximation with the recent dense plasma experiments for the He-like Cl ion between 600 eV and 650 eV [15] and the Al ion between 250 eV and 375 eV [14], respectively.

As we already pointed out earlier in Section 1, both IS models were able to generate the estimated redshifts that are in agreement with only one of the recent experimental measurements [14,15], but not the other. One possibility could be due to their application of the Fermi–Dirac statistics for the outside plasma. For many other theoretical approaches, the temperature dependence would also be implicitly determined by the free electron density expressed in terms of the Fermi–Dirac distributions. In contrast, for the DH model, the electrons and ions in the outside charge- neutral plasma are treated as charged particles with no quantum mechanical interaction (such as those involving the spin of the individual particles in the solid system or inside the nucleus), and thus, the Maxwell–Boltzmann statistics is applied. This is very different from the Fermi–Dirac distribution applied in the AIS model. It is interesting to note that a statistical electron screening model was proposed very recently [13] to describe the atomic processes in warm/hot dense plasmas

with a wide range of temperatures and densities. This model includes corrections for the Fermi–Dirac distribution by considering the non-equilibrium feature of the plasma electron distribution around the atomic ion caused by the three-body recombination process, which effectively broadened the phase space of the plasma electron and made the plasma electron distribution more close to the Boltzmann distribution under high temperatures. In fact, for the conditions relevant to the two recent experiments [14,15], such a sophisticated statistical model results in a plasma electron distribution almost identical to the DH model and can result in a similar conclusion as we presented earlier. Although there is no definitive quantitative measurement on the redshifts with different plasma temperatures at a fixed plasma density, the two recent experiments were carried out with a range of estimated temperatures that appeared to suggest a temperature dependence of energy shifts $\Delta\omega$ more pronounced than the fairly small variations at different temperatures obtained from the two versions of the IS model.
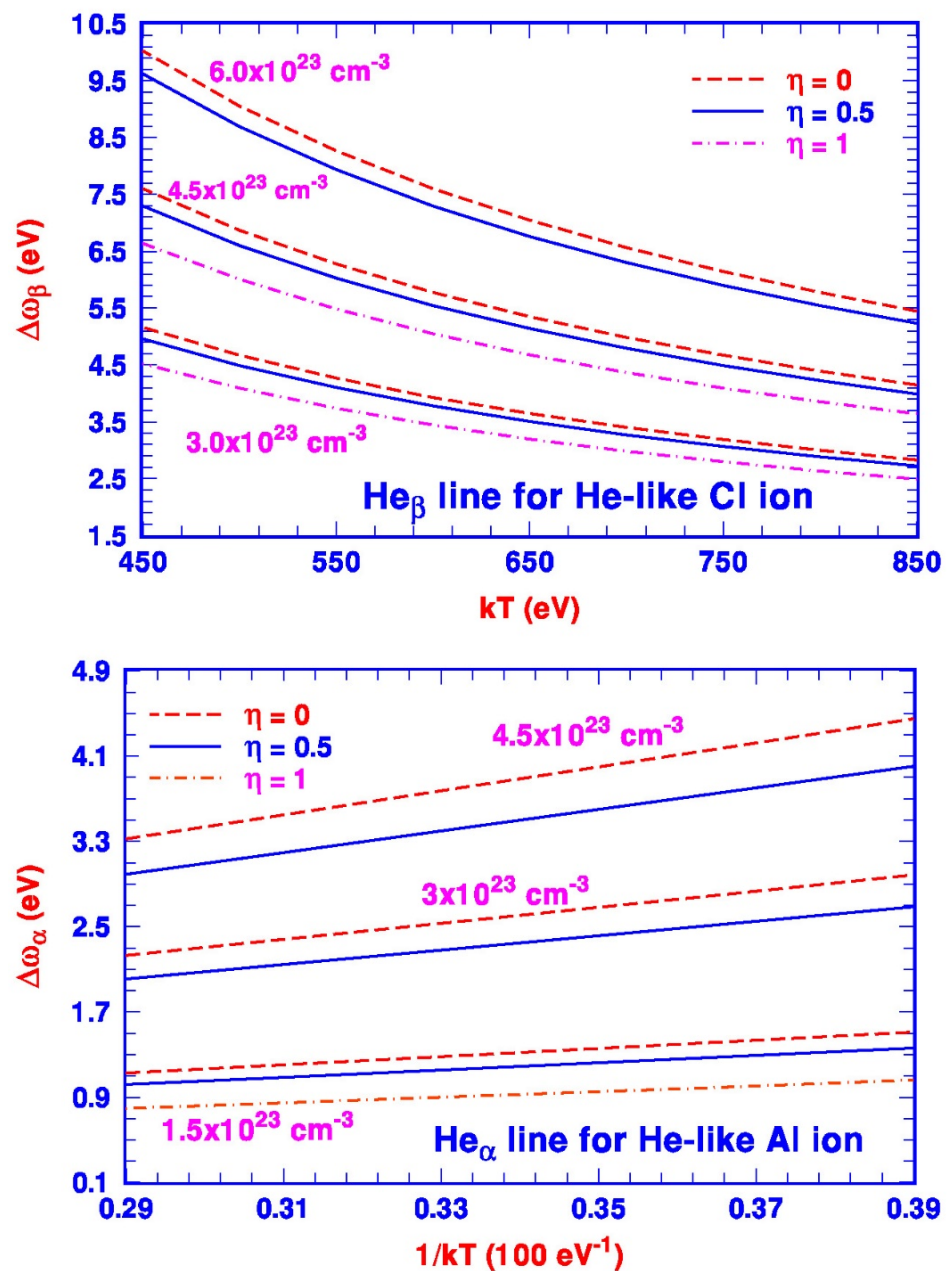

Figure 4. The theoretically estimated redshifts $\Delta\omega$ as functions of kT and $1/kT$ derived from Equation (17) at a number of plasma densities.

It is important to point out that the failure of the application of the DH model to an atomic process without taking into account appropriately the critical physical aspects of the spatial and temporal criteria should not invalidate the DH approximation as a viable phenomenological approach. For example, the DH approximation should not be applied at all to transitions involving atomic states close to the ionization threshold such as the "dip" shown near the series limit in Figure 2 of [49]. The other such example is due to the definition of the Debye length D. As we already pointed out earlier [20], some applications of the DH approximation have included an extra $(Z + 1)$ factor to the plasma density in defining the Debye length. This would lead to a smaller Debye length and consequently a much stronger plasma effect. One such example is shown by the large difference between the DH calculation and the results from other calculations shown in Figure 2 of the recent work by Gu and Beiersdorfer [50] due to the fact that their Debye length was over an order of magnitude smaller than what it should be at a given temperature. Once again, we would like to emphasize that the inability of generating reliable data based on questionable applications should not be viewed as the shortcoming of the DH model.

We should also comment briefly on the size factor η. There is no good a priori theoretical prescription to determine its value other than to assume the maximum plasma effect to the atomic electron when $\eta = 0$ and the calculated $\Delta\omega$ could be identified as the upper bound for the energy shifts. Based on the spatial criterion of the DH model of keeping as much of the atomic characteristic of the transition, together with the good agreement between our estimated $\Delta\omega$ with the measured data shown in Figure 3, a reasonable compromise would be for η to be close to 0.5, but less than one. Certainly, more high-precision experiments will help refine the choice of the size parameter η.

For the effect of the outside plasma on the oscillator strength f for the α and β emissions of the H-like and He-like ions, we focus our discussion similarly to those presented above in terms of its variation as a function of the reduced Debye length λ. Specifically, we examined the ratio f_r between the change in f and its plasma-free value $f(\lambda = \infty)$, i.e.,

$$f_r(\lambda) = \frac{f(\lambda = \infty) - f(\lambda)}{f(\lambda = \infty)}. \tag{18}$$

It is interesting to note from Figure 5 that our calculated percentage variation of the ratio f_r as a function of λ for the He$_\alpha$ line exhibits a similar qualitative feature as the ratio for the energy shift R discussed earlier. In other words, this general feature could also be expressed in terms of a polynomial, i.e.,

$$f_r(\lambda; a_f, b_f, c_f) = a_f + b_f/\lambda + c_f/\lambda^2. \tag{19}$$

We also note from Figure 5 that f_r is generally a few times larger than the value of R as a function of λ, or at the same temperature kT and density N. Even with R at a fraction of 1%, the energy resolution of the current experiments such as those we referred to earlier is sufficient to measure the energy shifts with reasonable accuracy. However, it may still be difficult to experimentally measure the change in the oscillator strength even at a level of a few percent change in f_r, as shown in Figure 5.
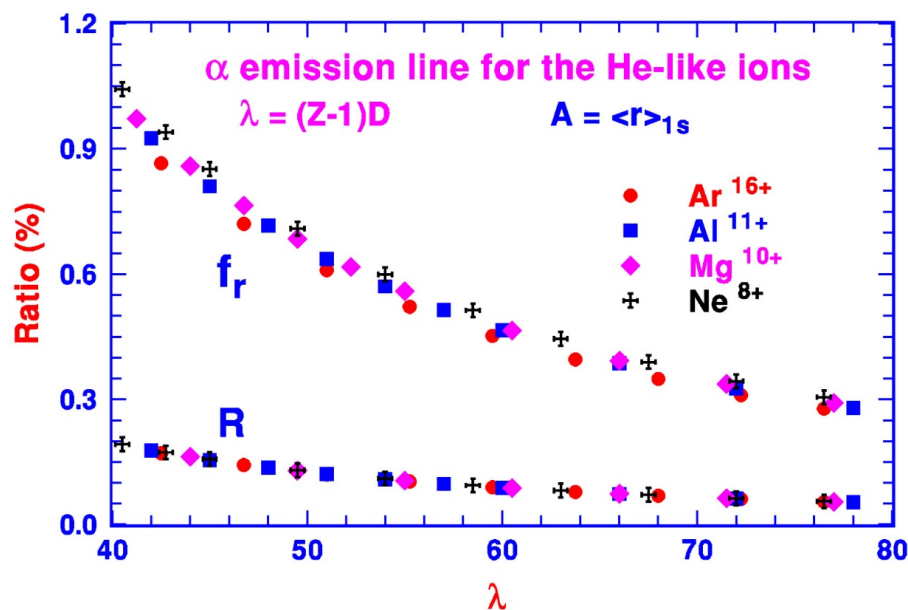
Figure 5. The percentage change of the redshifts R and the corresponding f_r of the oscillator strengths for the $1s2\,^1S \rightarrow 1s2p\,^1P$ transition of the He-like ions as a function of λ.

4. Photoabsorption

Our theoretical study on the atomic processes subject to the outside plasma actually started with the atomic photoionization from the ground states of the one- and two-electron atoms [19]. Experimentally, most of the photoionization measurements in the plasma-free environment are focused on the angular distribution of the outgoing photoelectrons, which offers more information to understand the detailed dynamics of the process either with the polarized or unpolarized incident light. In the presence of the outside plasma, the outgoing atomic electron resulting from the absorption of the incoming photon by the atom will lose its identity due to its interaction with the plasma electrons and accordingly could not be collected as the ones in the plasma-free environment. As a result, the experimental study of such a process would likely be limited to the measurement of the attenuation of the incident photon. In this section, we present our discussion of the qualitative feature of the photoabsorption process from the ground state of the one-electron atom, which meets the spatial criterion of the DH approximation.

For the hydrogen atom, the oscillator strength and its corresponding photoabsorption cross-section are proportional to the square of the dipole matrix element $< \chi_{1s}|r|\chi_{kp} >$, where χ are the solutions of the one-electron Hamiltonian h_o given by Equation (8) and $k^2 = \epsilon$ is the energy of the ionized p electron in Rydberg units with momentum k. Qualitatively, the larger the overlap between χ_{1s} and χ_{kp}, the greater the cross-section is. The radial parts of the wave function of the outgoing kp electron with slightly different energies near the ionization threshold for a plasma-free photoabsorption from the hydrogen atom are essentially the same as shown by the top plot of Figure 6 for a number of momenta k. They all reach their first local maxima and the subsequent zeros at about the same distance r and only differ from each other until they are sufficiently away from the nucleus at large r. Since the photoabsorption spectrum is dictated by the overlaps of the χ_{kp} with the $1s$ orbit up to a distance before the $1s$ orbit reaches zero (see, e.g., the bottom plot of Figure 6), only the close-in part of χ_{kp} at the relatively small r needs to be taken into account for the slowly varying dipole matrix element $< \chi_{1s}|r|\chi_{kp} >$ as the energy changes. This is consistent with the plasma-free hydrogen photoabsorption spectrum, which is known to vary smoothly near the ionization threshold [51]. We should point out that this short-range nature of the photoabsorption from the hydrogen ground state is necessary to meet the spatial criterion required in the application of the DH approximation in the presence of the outside plasma.
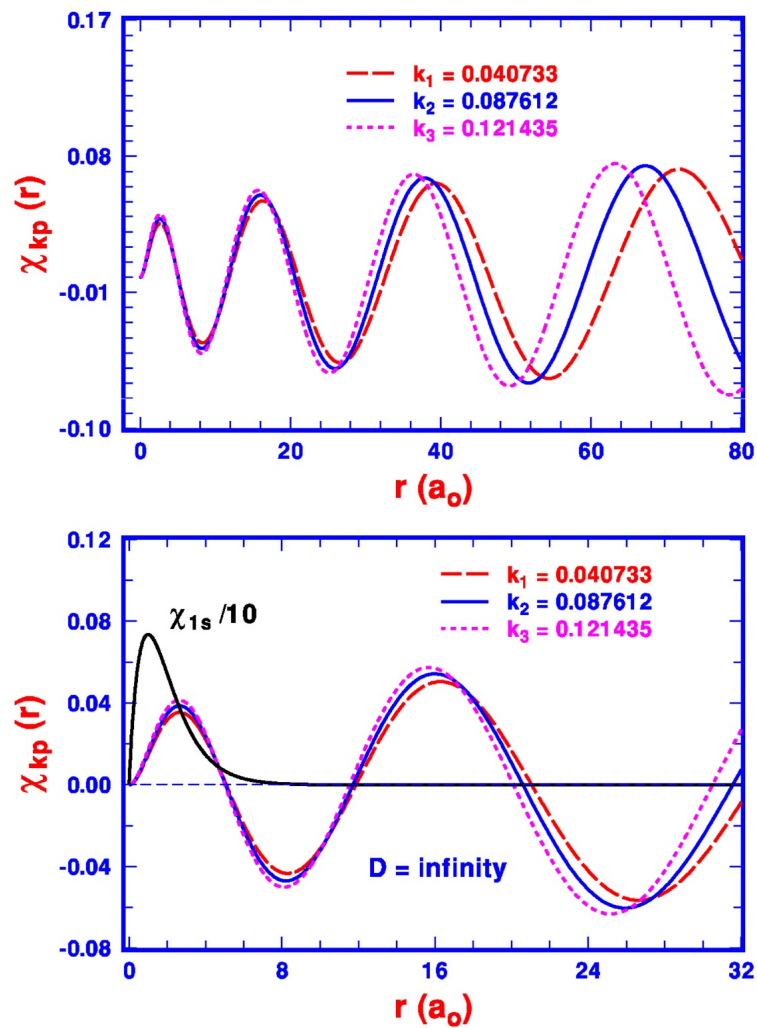
Figure 6. The radial functions χ_{kp} of the outgoing ionized p electron from the plasma-free hydrogen at a number of momenta. The bottom plot compares χ_{kp} to χ_{1s} (reduced by a factor of 10) at small r.

　　　We limit our detailed discussion on the application of the DH approximation to the photoabsorption of the hydrogen ground state subject to the plasma environment and examine first with the Debye lengths D substantially greater than the radius of the $1s$ orbital to keep the plasma effect on the the orbital wavefunction χ_{1s} small. Qualitatively, one of the most outstanding features of the DH approximation is the upwards migration of the bound excited state as the Debye length D decreases. Corresponding to each bound excited state, there is a critical value of D such that the state is pushed into the continuum. In particular, we focus our discussion on the plasma-induced resonant structures in the photoabsorption spectrum from the hydrogen ground state between 989 Åand 992 Å, which are associated with the plasma-free $1s$ to $4p$ Lyman-γ line at 972.5 Å. Following the earlier plasma-free example, but with the Debye length at a critical length of 24.5 a_o given in [19] due to the outside plasma, the top plot of Figure 7 compares the radial orbital function χ_{1s} to three χ_{kp} orbitals representing the outgoing electron near the ionization threshold at three momenta $k = 0.030301, 0.034244$, and 0.037739, respectively. It is interesting to note that although the locations of their first local maxima and the subsequent zeros for the first loop from $r = 0$ for all three χ_{kp} are similar to the plasma-free ones shown in Figure 6, their magnitudes are very different as k varies. At $k = 0.030301$ and 0.037739, the magnitudes of their first loop are relatively small, indicating a minimal presence of the outgoing electron at the inner region of the atom, similar to those shown in Figure 6 for the plasma-free photoabsorption. At a slightly different energy with $k = 0.034244$, the magnitude of χ_{kp} is noticeably higher at small r, but relatively small at larger r compared to that of the two

other momenta, indicating the presence of a quasi-bound radial wavefunction. As a result, its corresponding photoabsorption cross-section σ proportional to the square of the dipole matrix $|<\chi_{1s}|r|\chi_{kp}>|^2$ is substantially larger than those at the nearby k, leading to a resonant structure in the photoabsorption spectrum such as the one shown in the top plot of Figure 8 with $D = 24.5a_o$ at $kT = 600$ eV and $N = 1.973 \times 10^{22}$ cm^{-3}. Two additional narrow resonant structures due to slightly larger critical Debye lengths are also shown. It is interesting to note that the relative locations of the peak cross-sections of these three narrow resonant structures are expected under the DH approximation. This is due to the fact that the ionization threshold corresponding to a smaller Debye length is smaller than the one with a larger Debye length, and it requires less photon energy (or a longer wavelength) to "push" the 1s to 4p transition into the continuum. A similar feature due to the hydrogen 1s to 3p transition was also discussed in detail in [52]. With the electron–electron correlation between atomic electrons taken into account fully for the He atom, our study [19] also led to a similar general feature of the narrow resonance-like structure slightly above the changing ionization threshold in the photoabsorption spectrum. In spite of our theoretical understanding of the general feature of the plasma driving narrow resonances due to the migration of the excited np levels into the continuum in the photoabsorption process, unfortunately, the widths of such resonances are approximately 10,000-times smaller than the photon energy and likely not observed in the laboratory.
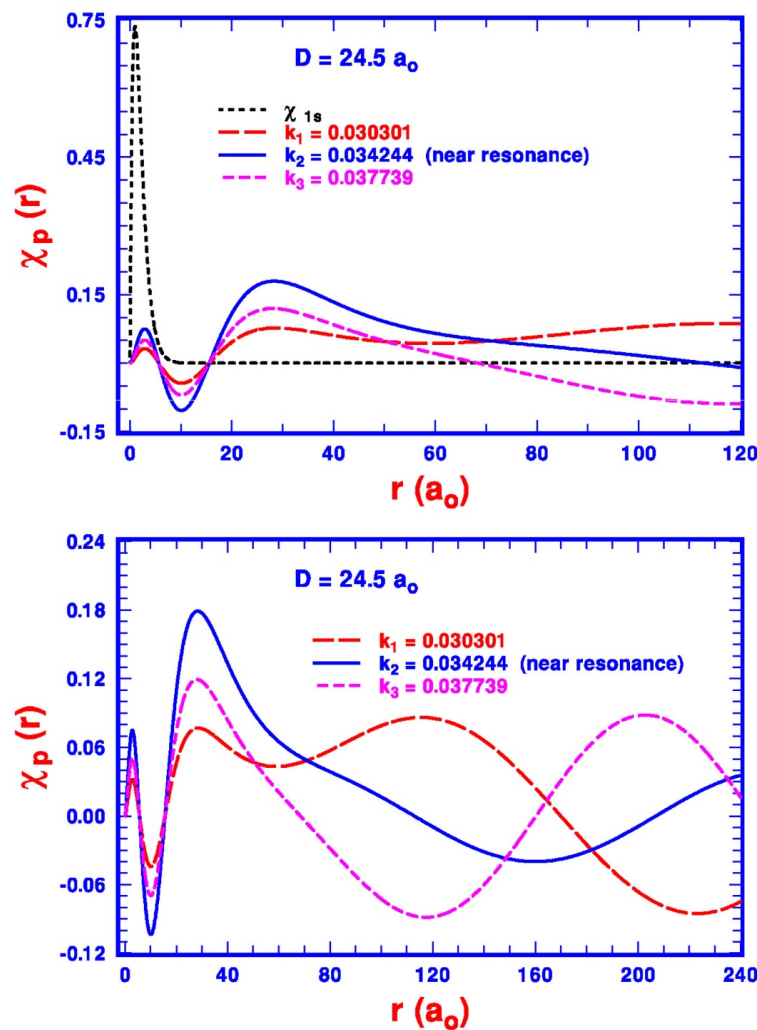
Figure 7. The top plot compares the radial functions χ_{kp} of the outgoing ionized p electron to χ_{1s} for hydrogen ground state photoabsorption subject to the outside plasma with $D = 24.5a_o$. The bottom figure shows an enlarged plot of χ_{kp} with an expanded scale up to $r = 240a_o$.
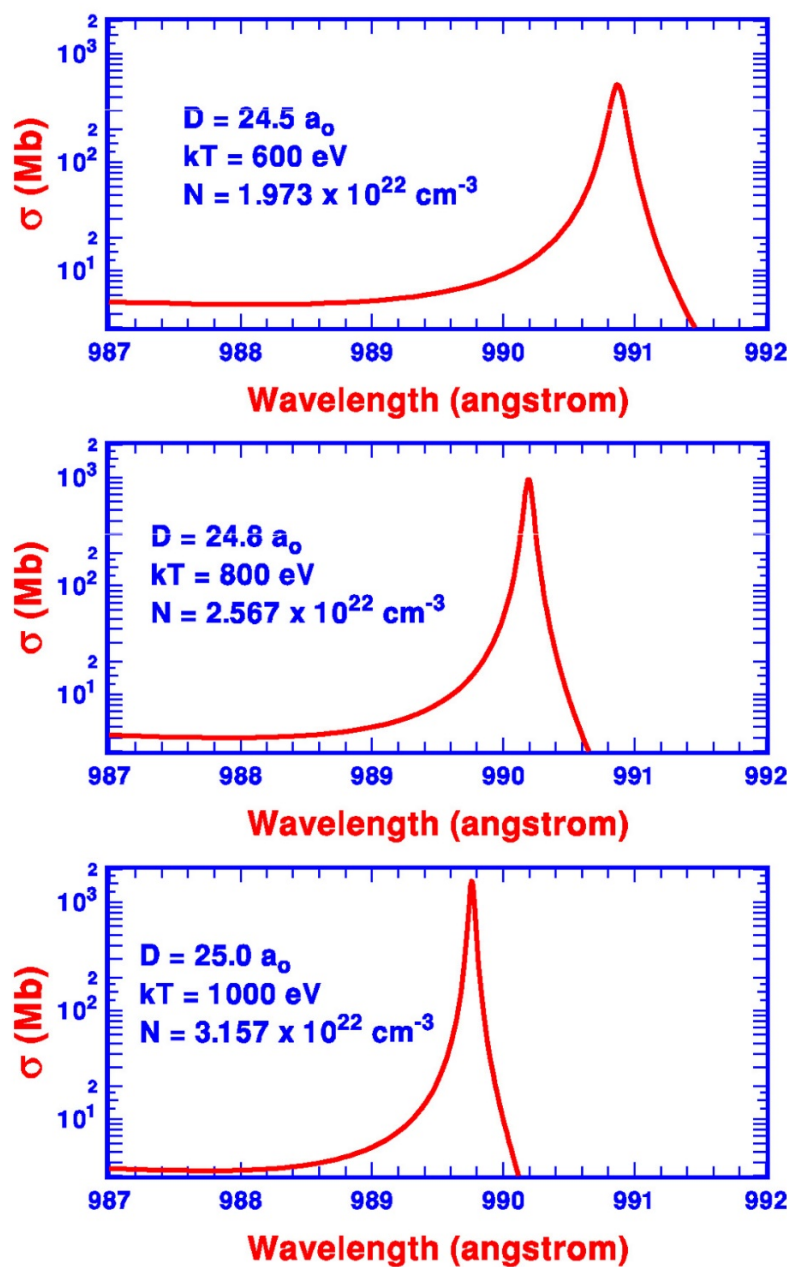
Figure 8. Hydrogen photoabsorption spectra from its ground state in terms of the cross-section σ (in units of Mb) corresponding to the $1s \rightarrow 4p$ transition as D varies around $24.5a_o$ with $A = 0$.

5. Conclusions

We presented in this paper a review of a series of our recent studies on the application of the Debye–Hückel approximation for atomic processes subject to the outside plasma environment. We focused our studies primarily on the processes that meet the all important spatial and temporal criteria for the DH model. In spite of the simplicity of the DH approximation, our theoretical results compared well with the limited data from the available experimental measurements. In addition, we identified a general scaling feature for the ratio R between the redshift $\Delta\omega$ and the plasma-free transition energy ω_0 of the α and β emission lines of the He-like ions with the nuclear charge Z between six and eighteen. More specifically, the ratio R could be expressed in terms of a simple polynomial Equation (17) of the reduced Debye length λ. Following the simple three-step procedure presented in Section 3, one could estimate the redshifts of the α or β emission lines for other He-like ions with no need for additional theoretical calculations. In fact, one such

example led to good agreement between the estimated redshifts of the β emission line for the He-like Cl ion and the experimental data shown in Figure 3.

In addition to our studies on the H- and He-like ions, we were also interested in finding out if the simple scaling feature presented in Section 3 also works for ions with more electrons. Our first such study was for the 3C and 3D lines of the Ne-like ions [53]. It turned out that for the dipole-allowed 3C line, the redshifts of the transition energy and the oscillator strength follow a similar scaling feature. However, for the dipole-forbidden 3D line, due to the interplay between the relativistic spin–orbit interaction and the plasma screening effects, the simple scaling feature failed to follow [53]. Following our study for the transitions for the Ne-like ions, we extended our study to two strong dipole transitions for the C-like ions, i.e., (1) the intershell $2s^22p3d\ ^3D_1 \rightarrow 2s^22p^2\ ^3P_0$ transition and (2) the intrashell $2s2p^3\ ^3D_1 \rightarrow 2s^22p^2\ ^3P_0$ transition. For the intrashell transition, the ratio of the energy shifts to its plasma-free transition energy and the increase of the oscillator strength follows a similar general scaling property. However, due to the change of the electron correlation with respect to the relativistic spin–orbit interaction as Z varies, the decrease in the oscillator strength for the intershell transition failed to follow the scaling feature discussed earlier [54].

Finally, we should comment again on the size factor η. As we stated earlier that there is no good a priori theoretical prescription to determine its value, therefore, the most appropriate η for the theoretical calculation would depend on the good agreement between the theoretically calculated $\Delta\omega$ and the measured data such as those shown in Figure 3. The interplay between the theory and experiment could refine the value of η and offer a more reliable and accurate determination of the energy shifts of the emission lines at a given combination of plasma temperature and density. In addition, as we indicated earlier that although the temperature variation of $\Delta\omega$ at a fixed plasma density based on the limited experimental date appears to support the use of the classical Maxwell–Boltzmann statistics over the Fermi–Dirac distributions for the outside plasma, more experimental measurements are needed for such a conclusion.

Institutional Review Board Statement: Not applicable.

Informed Consent Statement: Not applicable.

Data Availability Statement: Not applicable.

Conflicts of Interest: The authors declare no conflict of interest.

Abbreviations

The following abbreviations are used in this manuscript:

DH	Debye–Hückel
IS	Ion sphere
AIS	Average atom ion sphere
BSCI	B-spline-based configuration interaction

CSFs	Configuration state functions
AOs	Atomic orbital wave functions
MCDF	Multiconfiguration Dirac–Fock
QMIT	Quantum mechanical impact theory

References

1. Tennyson, J. *Astronomical Spectroscopy: An Introduction to the Atomic and Molecular Physics of Astronomical Spectral*; Press Imperial College: London, UK, 2005. [CrossRef]
2. Kallman, T.R.; Palmeri, P. Atomic data for x-ray astrophysics. *Rev. Mod. Phys.* **2007**, *79*, 79–133. [CrossRef]
3. Lindl, J.D.; Amendt, P.; Berger, R.L.; Glendinning, S.G.; Glenzer, S.H.; Haan, S.W.; Kauffman, R.L.; Landen, O.L.; Suter, L.J. The physics basis for ignition using indirect-drive targets on the National Ignition Facility. *Phys. Plasmas* **2004**, *11*, 339–491. [CrossRef]
4. Boozer, A.H. Physics of magnetically confined plasmas. *Rev. Mod. Phys.* **2005**, *76*, 1071–1141. [CrossRef]
5. Koenig, M.; Malnoult, P.; Nguyen, H. Atomic structure and line broadening of He-like ions in hot and dense plasmas. *Phys. Rev. A* **1988**, *38*, 2089–2098. [CrossRef] [PubMed]
6. Nguyen, H.; Koenig, M.; Benredjem, D.; Caby, M.; Coulaud, G. Atomic structure and polarization line shift in dense and hot plasmas. *Phys. Rev. A* **1986**, *33*, 1279–1290. [CrossRef] [PubMed]
7. Davis, J.; Blaha, M. Level shifts and inelastic electron scattering in dense plasmas. *J. Quant. Spectrosc. Radiat. Transf.* **1982**, *27*, 307–313. [CrossRef]
8. Li, X.; Rosmej, F.B. Quantum-number dependent energy level shifts of ions in dense plasmas: A generalized analytical approach. *Europhys. Lett.* **2012**, *99*, 33001. [CrossRef]
9. Rosmej, F.; Bennadji, K.; Lisitsa, V.S. Effect of dense plasmas on exchange-energy shifts in highly charged ions: An alternative approach for arbitrary perturbation potentials. *Phys. Rev. A* **2011**, *84*, 032512. [CrossRef]
10. Chen, Z.B. Calculation of the energies and oscillator strengths of Cl^{15+} in hot dense plasmas. *J. Quant. Spectrosc. Radiat. Transf.* **2019**, *237*, 106615. [CrossRef]
11. Glenzer, S.H.; Redmer, R. X-ray Thomson scattering in high energy density plasmas. *Rev. Mod. Phys.* **2009**, *81*, 1625–1663. [CrossRef]
12. Ichimaru, S. Strongly coupled plasmas: High-density classical plasmas and degenerate electron liquids. *Rev. Mod. Phys.* **1982**, *54*, 1017–1059. [CrossRef]
13. Zhou, F.; Qu, Y.; Gao, J.; Ma, Y.; Wu, Y.; Wang, J. Atomic-state-dependent screening model for hot and warm dense plasmas. *Commun. Phys.* **2021**, *4*, 148. [CrossRef]
14. Stillman, C.R.; Nilson, P.M.; Ivancic, S.T.; Golovkin, I.E.; Mileham, C.; Begishev, I.A.; Froula, D.H. Picosecond time-resolved measurements of dense plasma line shifts. *Phys. Rev. E* **2017**, *95*, 063204. [CrossRef]
15. Beiersdorfer, P.; Brown, G.V.; McKelvey, A.; Shepherd, R.; Hoarty, D.J.; Brown, C.R.D.; Hill, M.P.; Hobbs, L.M.R.; James, S.F.; Morton, J.; et al. High-resolution measurements of Cl^{15+} line shifts in hot, solid-density plasmas. *Phys. Rev. A* **2019**, *100*, 012511. [CrossRef]
16. Chen, Z.B.; Wang, K. Theoretical study on the line shifts of He-like Al11+ ion immersed in a dense plasma. *Radiat. Phys. Chem.* **2020**, *172*, 108816. [CrossRef]
17. Debye, P.; Hückel, E. The theory of electrolytes I. The lowering of the freezing point and related occurrences. *Phys. Z.* **1923**, *24*, 185–206.
18. Chen, F.F. *Introduction to Plasma Physics and Controlled Fusion Plasma Physics*; Springer International Publishing: Cham, Switzerland, 2016. [CrossRef]
19. Chang, T.N.; Fang, T.K. Atomic photoionization in a changing plasma environment. *Phys. Rev. A* **2013**, *88*, 023406. [CrossRef]
20. Chang, T.N.; Fang, T.K.; Gao, X. Redshift of the Lyman-α emission line of H-like ions in a plasma environment. *Phys. Rev. A* **2015**, *91*, 063422. [CrossRef]
21. Fang, T.K.; Wu, C.S.; Gao, X.; Chang, T.N. Redshift of the He α emission line of He-like ions under a plasma environment. *Phys. Rev. A* **2017**, *96*, 052502. [CrossRef]
22. Fang, T.K.; Wu, C.S.; Gao, X.; Chang, T.N. Variation of the oscillator strengths for the α emission lines of the one- and two-electrons ions in dense plasma. *Phys. Plasmas* **2018**, *25*, 102116. [CrossRef]
23. Chang, T.N.; Fang, T.K.; Wu, C.S.; Gao, X. Redshift of the isolated atomic emission line in dense plasma. *Phys. Scr.* **2021**, *96*, 124012. [CrossRef]
24. Mukherjee, P.K.; Karwowski, J.; Diercksen, G.H.F. On the influence of the Debye screening on the spectra of two-electron atoms. *Chem. Phys. Lett.* **2002**, *363*, 323–327. [CrossRef]
25. Sil, A.N.; Mukherjee, P.K. Effect of debye plasma on the doubly excited states of highly stripped ions. *Int. J. Quantum Chem.* **2005**, *102*, 1061–1068. [CrossRef]
26. Zhang, S.B.; Wang, J.G.; Janev, R.K. Electron-Hydrogen-atom elastic and inelastic scattering with screened Coulomb interaction around the n = 2 excitation threshold. *Phys. Rev. A* **2010**, *81*, 032707. [CrossRef]
27. Zhang, S.B.; Wang, J.G.; Janev, R.K. Crossover of feshbach resonances to shape-type resonances in electron-hydrogen atom excitation with a screened Coulomb interaction. *Phys. Rev. Lett.* **2010**, *104*, 023203. [CrossRef] [PubMed]

28. Qi, Y.Y.; Wu, Y.; Wang, J.G.; Qu, Y.Z. The generalized oscillator strengths of Hydrogenlike ions in Debye plasmas. *Phys. Plasmas* **2009**, *16*, 023502. [CrossRef]

29. Dai, S.T.; Solovyova, A.; Winkler, P. Calculations of properties of screened He-like systems using correlated wave functions. *Phys. Rev. E* **2001**, *64*, 016408. [CrossRef] [PubMed]

30. Lopez, X.; Sarasola, C.; Ugalde, J.M. Transition energies and emission oscillator strengths of Helium in model plasma environments. *J. Phys. Chem. A* **1997**, *101*, 1804–1807. [CrossRef]

31. Kar, S.; Ho, Y.K. Oscillator strengths and polarizabilities of the hot-dense plasma-embedded Helium atom. *J. Quant. Spectrosc. Radiat. Transf.* **2008**, *109*, 445–452. [CrossRef]

32. Kar, S.; Ho, Y.K. Photodetachment of the Hydrogen negative ion in weakly coupled plasmas. *Phys. Plasmas* **2008**, *15*, 013301. [CrossRef]

33. Shukla, P.K.; Eliasson, B. Screening and wake potentials of a test charge in quantum plasmas. *Phys. Lett. A* **2008**, *372*, 2897–2899. [CrossRef]

34. Kar, S.; Ho, Y.K. Electron affinity of the Hydrogen atom and a resonance state of the Hydrogen negative ion embedded in Debye plasmas. *New J. Phys.* **2005**, *7*, 141. [CrossRef]

35. Ghoshal, A.; Ho, Y.K. Ground states and doubly excited resonance states of H^- embedded in dense quantum plasmas. *J. Phys. B-At. Mol. Opt. Phys.* **2009**, *42*, 175006. [CrossRef]

36. Saemann, A.; Eidmann, K.; Golovkin, I.E.; Mancini, R.C.; Andersson, E.; Förster, E.; Witte, K. Isochoric heating of solid Aluminum by ultrashort laser pulses focused on a tamped target. *Phys. Rev. Lett.* **1999**, *82*, 4843–4846. [CrossRef]

37. Margenau, H.; Lewis, M. Structure of spectral lines from plasmas. *Rev. Mod. Phys.* **1959**, *31*, 569–615. [CrossRef]

38. Rouse, C.A. Finite Electronic Partition Function from Screened Coulomb Interactions. *Phys. Rev.* **1967**, *163*, 62–71. [CrossRef]

39. Chang, T.N. B-Spline Based Configuration-Interaction Approach for Photoionization of Two-electron and Divalent Atoms. In *Many-Body Theory of Atomic Structure and Photoionization*; World Scientific: Singapore, 1993; pp. 213–247. [CrossRef]

40. Chang, T.N.; Tang, X. Photoionization of two-electron atoms using a nonvariational configuration-interaction approach with discretized finite basis. *Phys. Rev. A* **1991**, *44*, 232–238. [CrossRef]

41. Chang, T.N. Application of the many-body theory of atomic transitions to the photoionization of neon and argon. *Phys. Rev. A* **1977**, *15*, 2392–2395. [CrossRef]

42. Chang, T.N.; Fano, U. Many-body theory of atomic transitions. *Phys. Rev. A* **1976**, *13*, 263–281. [CrossRef]

43. Grant, I.P. *Relativistic Quantum Theory of Atoms and Molecules*; Springer: New York, NY, USA, 2007. [CrossRef]

44. Jönsson, P.; Gaigalas, G.; Bieron, J.; Fischer, C.F.; Grant, I.P. New version: GRASP2K relativistic atomic structure package. *Comput. Phys. Commun.* **2013**, *184*, 2197–2203. [CrossRef]

45. Han, X.Y.; Gao, X.; Zeng, D.l.; Jin, R.; Yan, J.; Li, J.M. Scaling law for transition probabilities in $2p^3$ configuration from LS coupling to jj coupling. *Phys. Rev. A* **2014**, *89*, 042514. [CrossRef]

46. Gao, X.; Han, X.Y.; Zeng, D.L.; Jin, R.; Li, J.M. Broken scaling laws of the transition probabilities from jj to LS coupling transitions. *Phys. Lett. A* **2014**, *378*, 1514–1519. [CrossRef]

47. Han, X.Y.; Gao, X.; Zeng, D.L.; Yan, J.; Li, J.M. Ratio of forbidden transition rates in the ground-state configuration of O II. *Phys. Rev. A* **2012**, *85*, 062506. [CrossRef]

48. Kramida, A.; Ralchenko, Y.; Reader, J.; Team, N.A. *NIST Atomic Spectra Database (Ver. 5.8)*; National Institute of Standards and Technology: Gaithersburg, MD, USA, 2020. Available online: https://physics.nist.gov/asd (accessed on 11 October 2021).

49. Nantel, M.; Ma, G.; Gu, S.; Côté, C.Y.; Itatani, J.; Umstadter, D. Pressure ionization and line merging in strongly coupled plasmas produced by 100-fs laser pulses. *Phys. Rev. Lett.* **1998**, *80*, 4442–4445. [CrossRef]

50. Gu, M.F.; Beiersdorfer, P. Stark shift and width of x-ray lines from highly charged ions in dense plasmas. *Phys. Rev. A* **2020**, *101*, 032501. [CrossRef]

51. Marr, G.V. *Photoionization Processes in Gases*; Academic Press: New York, NY, USA, 1967.

52. Chang, T.N.; Fang, T.K.; Ho, Y.K. One- and two-photon ionization of hydrogen atom embedded in Debye plasmas. *Phys. Plasmas* **2013**, *20*, 092110. [CrossRef]

53. Wu, C.S.; Chen, S.M.; Chang, T.N.; Gao, X. Variation of the transition energies and oscillator strengths for the 3C and 3D lines of the Ne-like ions under plasma environment. *J. Phys. B-At. Mol. Opt. Phys.* **2019**, *52*, 185004. [CrossRef]

54. Wu, C.S.; Wu, Y.; Yan, J.; Chang, T.N.; Gao, X. Transition energies and oscillator strengths for the intrashell and intershell transitions of the C-like ions in a thermodynamic equilibrium plasma environment. *Phys. Rev. E* **2022**, *105*, 015206. [CrossRef]